Iraqi Journal of Physics, 2021 *Vol.19, No.48, PP. 21-32*

DOI: 10.30723/ijp.19.48.21-32

Study of the Proton Halo Structure of Nuclei ^{23}Al and ^{27}P Using the Binary Cluster Model

Luay F. Sultan, Ahmed N. Abdullah

Department of Physics, College of Science, University of Baghdad, Baghdad, Iraq

E-mail: Ahmednajem2018@gmail.com

Corresponding author: luayfadhil1991@gmail.com

Abstract

The Binary Cluster Model (BCM) was employed within the single particle wave functions of Gaussian and harmonic oscillator potentials to study the ground state density distributions of proton-rich ^{23}Al and ^{27}P halo nuclei. The long tail performance was clearly noticed in the calculated proton and matter density distributions of these nuclei. Elastic form factors of these exotic nuclei were studied by the Plane Wave Born Approximation (PWBA). It were found that the major difference between the calculated form factors of unstable nuclei [^{23}Al, ^{27}P] and those of their stable isotopes [^{27}Al, ^{31}P] is caused by the variation in the proton density distributions, especially the details of the outer part. Moreover, the matter root-mean-square (rms) radii and reaction cross sections for these exotic nuclei were studied by means of the Glauber model with an optical limit approximation using the ground state densities of the projectile and target, where these densities are described by single Gaussian functions. The calculated results of rms radii and reaction cross sections were in good agreement with the data.

Key words

Glauber model, exotic nuclei, binary cluster model, Proton-rich nuclei.

Article info.

Received: Sep. 2020
Accepted: Dec. 2020
Published: Mar. 2021

دراسة تركيب الهالة البروتوني للنوى ^{23}Al و ^{27}P باستخدام الانموذج العنقودي الثنائي

لؤي فاضل سلطان، احمد نجم عبدالله

قسم الفيزياء، كلية العلوم، جامعة بغداد، بغداد، العراق

الخلاصة

تم استخدام الأنموذج العنقودي الثنائي مع الدوال الموجية للجسيمة المفردة لجهدي جاوس والمتذبذب التوافقي لدراسة توزيعات الكثافة للحالة الارضية لنوى الهالة الغنية بالبروتونات ^{23}Al و ^{27}P. الامتداد الطويل ظهر بوضوح في توزيعات الكثافة البروتونية والكتلية لهذه النوى. عوامل التشكل المرنة لهذه النوى تم دراستها بواسطة تقريب بورن للموجة المستوية. وجد ان الاختلاف بين عوامل التشكل للنوى الغريبة [^{27}P, ^{23}Al] ونظيرتها المستقرة [^{31}P, ^{27}Al] يعود الى التباين في توزيعات الكثافة البروتونية لهذه النوى والناتج بصورة رئيسية من وجود بروتون في مدارات الهالة. انصاف الاقطار النووية المادية والمقاطع العرضية للتفاعل لهذه النوى تم دراستها باستخدام نموذج گلوبر باستخدام توزيع الكثافة للحالة الارضية للنواة القذيفة والهدف، حيث ان هذه الكثافات توصف بواسطة دوال گاوس للجسيمة المنفردة. النتائج المحسوبة لانصاف الاقطارالنووية والمقاطع العرضية للتفاعل لهذه النوى تتفق بشكل جيد مع القيم العملية.

Introduction

Since the discovery of neutron halo in exotic light neutron-rich nuclei in the mid-eighties [1, 2], studies on halo phenomena have become a hot point in nuclear physics. The neutron halo is a weakly bound exotic nuclear state where the valence

neutrons are spatially decoupled from a tightly bound core and the wave function extends into the classically forbidden region [3]. The cause of halo phenomena lies in both the small separation energy of the last few nucleons and their occupation on the orbits with low angular momentum (l = 0, 1) [4], which allow the wave function of the valence nucleons to extend to large radii [5].

Many experiments [6-9] have been performed to study neutron halo in neutron-rich nuclei. Neutron-halo nuclei are well identified in light mass region. Theoretically neutron halo in exotic nuclei ^{6,8}He, ^{11}Li, ^{11,14}Be, ^{17}B, and ^{19}C have also been well reproduced by various theoretical models [10-13]. Although neutron halo has been well investigated in neutron-rich nuclei, studies on proton halo are relatively few. Theoretically, much effort has been made to the search of proton halo in proton drip-line nuclei. Calculations showed that there may be proton halo in ^{26,27,28}P, ^{8}B and ^{17}Ne [14-17]. Experiments also showed some indications of the existence of proton halo in these nuclei [18-20]. However, further experiments are needed to confirm the existence of the proton halo. Thus, the proton halo phenomenon is a very interesting subject of investigation.

The total reaction cross section (σ_R) is one of the most important physical quantities characterizing the properties of nuclear reaction [21, 22]. It is very useful for extracting fundamental information about the nuclear size and the density distributions of neutrons and protons in a nucleus. In particular, the neutron halo was found by measuring the total reaction cross section induced by radioactive nuclear beams [1]. The reaction cross section is defined by the interaction cross sections plus the inelastic scattering cross sections ($\sigma_R = \sigma_I + \sigma_{inela}$) [23]. At high energy (above several hundred MeV/nucleon), it is known that the σ_R is approximated by σ_I ($\sigma_R \approx \sigma_I$) because the contribution of the inelastic scattering is low [24, 25].

Alzubadi et al. [26] calculated the mass density distributions, the associated nuclear radii and elastic electron scattering form factors of light exotic nuclei, ^{11}Li, ^{11}Be, ^{14}Be and ^{8}B using shell model (SM) and Hartree–Fock (HF) methods. They considered truncated *spsdpf* no-core SM and WBP two-body effective interaction to give the SM wave functions. The single-particle matrix elements was calculated with Skyrme–Hartree–Fock (SHF) potential with different parametrizations. It was shown that the calculated densities and form factors were in good agreement with the experimental data. This agreement can be interpreted as the adequacy of the HF mean-field approximation for exotic nuclei. Zhang et al. [18] performed measurements of σ_R for 44 nuclei with A<30 (mostly proton-rich), on carbon at intermediate energies by a transmission method. Their experimental σ_R values for ^{23}Al and ^{27}P were abnormally large compared with their neighboring nuclei. This suggested anomalously large matter rms radii and proton halo structure in ^{23}Al and ^{27}P. Ren *et al*. (2003) [27] performed measurement of the reaction cross section of N = 10 isotones and Z = 13 isotopes at Lanzhou in China. An abnormal increase in the reaction cross section was observed for ^{23}Al. This abnormal increase strongly suggests that there is a proton halo in ^{23}Al. Radhi et al. [28] used the two-frequency shell model approach to calculate the ground state matter density distribution and the corresponding root mean square radii of the two-proton^{17}Ne halo nucleus with the assumption that the model space of ^{15}O core nucleus differ from the model space of extra two loosely bound valence protons. Two different size parameters b_{core} and b_{halo} of the single particle wave functions of the harmonic oscillator potential were used. The calculations were carried out for different configurations of the outer halo protons in ^{17}Ne nucleus. The structure of this halo nucleus shows that the dominant configuration when the two halo protons in the $1d_{5/2}$ orbit (^{15}O core plus two protons

halo in pure $1d_{5/2}$ orbit). The calculated matter density distribution in terms of the two-frequency shell model was compared with the calculated one in terms one size parameter for all orbits to illustrate the effect of introducing one or two size parameters in calculations. Abdullah [29] studied the nuclear structure of proton halo nuclei ^{8}B, ^{17}Ne, ^{23}Al and ^{27}P using the SKxs25 parameterization within the Skyrme–Hartree–Fock (SHF) method. He found that this Skyrme parameters within the SHF method gave a good description of the nuclear structure of these proton halo nuclei.

In the present work, we shall use the binary cluster model (BCM) within the Gaussian and harmonic oscillator wave functions to study some of the basic structural properties such as the ground state proton, neutron and matter densities and elastic form factors for the proton-rich ^{123}Al and ^{27}P exotic nuclei. We shall also study the matter root-mean-square (rms) radii and reaction cross sections for these nuclei using the Glauber model with an optical limit approximation.

Theory

In BCM [30], the exotic halo nuclei are considered as composite projectiles of mass A_p and described, in Fig.1, as core and valence clusters, of masses A_c and A_v bounded with a state of relative motion. It is assumed that $A_c \geq A_v$. The matter density of the composite projectile is given by [31]:

$$\boldsymbol{\rho_m(r) = \rho_c(r) + \rho_v} \qquad (\mathbf{1})$$

Where $\rho_c(r)$ and $\rho_v(r)$ are the core and valence (halo) densities, respectively.
In this study, two density parameterizations are used namely; Gaussian (GS) and harmonic oscillator (HO) parameterizations
In the GS parameterization, density distributions of the core and halo clusters are parameterized with Gaussian wave function [30]:

$$\boldsymbol{\rho_m(r) = A_c\, g^{(3)}(\hat{\alpha}_c, r) + A_v\, g^{(3)}(\hat{\alpha}_v, r),} \qquad (\mathbf{2})$$

where $g^{(3)}$ is the normalized 3-dimensional Gaussian function given by the following equation [30]:

$$\boldsymbol{g^{(3)}\left(\hat{\alpha}_{c(v)}, r\right) = \frac{1}{\pi^{3/2}\hat{\alpha}^3_{c(v)}}\, e^{-r^2/\hat{\alpha}^2_{c(v)}}, \qquad \int g^{(3)}\left(\alpha_{c(v)}, r\right) d\vec{r} = 1} \quad (\mathbf{3})$$

whereas in the HO parameterization, density distributions of the core and halo clusters are parameterized with HO wave function as [32]:

$$\boldsymbol{\rho_c(r) = \frac{1}{4\pi}\sum_{n\ell} X_c^{n\ell}\left|R_{n\ell}(r, \hat{b}_c)\right|^2} \qquad (\mathbf{4})$$

$$\boldsymbol{\rho_v(r) = \frac{1}{4\pi} X_v^{n\ell}\left|R_{n\ell}(r, \hat{b}_v)\right|^2} \qquad (\mathbf{5})$$

The Gaussian $\left(\hat{\alpha}_c{}^2,\ \hat{\alpha}_v{}^2\right)$ and HO $\left(\hat{b}_c{}^2,\ \hat{b}_v{}^2\right)$ size parameters are given by [30, 31]:

$$\boldsymbol{\hat{g}_c{}^2 = g_c{}^2 + \left(\frac{A_v g}{A_v + A_c}\right)^2, \quad \hat{g}_v{}^2 = g_v{}^2 + \left(\frac{A_c g}{A_v + A_c}\right)^2, \quad g \equiv \alpha, b} \quad (\mathbf{6})$$

The matter density of Eq. (1) can be written as [33]:

$$\boldsymbol{\rho_m(r) = \rho^n(r) + \rho^p(r)} \qquad (\mathbf{7})$$

Where $\rho^n(r)$ and $\rho^p(r)$ are the neutron and proton densities, respectively written as [33]:

$$\boldsymbol{\rho^n(r) = \rho_c^n(r) + \rho_v^n(r)} \qquad (\mathbf{8})$$

and

$$\boldsymbol{\rho^p(r) = \rho_c^p(r) + \rho_v^p(r)} \qquad (\mathbf{9})$$

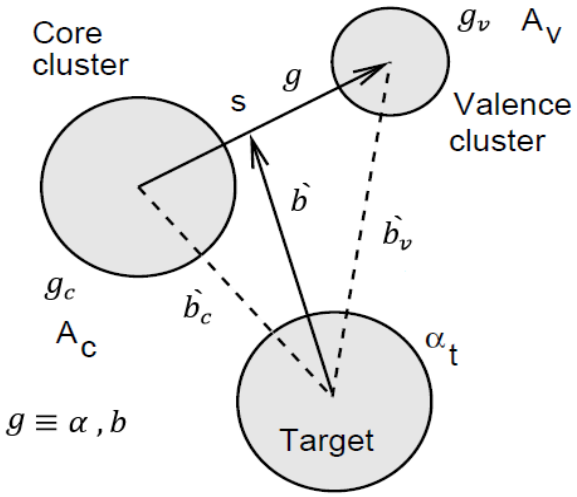

Fig.1: The coordinates of the target and two-cluster projectile [30].

The plane wave Born approximation (PWBA) within the proton density distribution obtained by HO parameterization is used to study the elastic form factors for the selected nuclei. The elastic form factor, in the PWBA, is given by [34]:

$$\boldsymbol{F(q) = \frac{4\pi}{Z}\int_0^\infty \rho_p(r) j_0(qr) r^2 dr,} \qquad \textbf{(10)}$$

Where $j_0(qr)$ and q are the zero-order spherical Bessel function and momentum transfer to the target nucleus from the incident electron, respectively.

One of the widely used models for analyzing the interaction and the reaction cross sections of nucleus-nucleus scattering is the Glauber model [35]. The reaction cross section (σ_R) using the Glauber model within an Optical Limit Approximation (OLA) can be expressed as [36]:

$$\boldsymbol{\sigma_R = 2\pi \int [1 - T(b)]\, b\, db \left(1 - \frac{B_c}{E_{cm}}\right)} \qquad \textbf{(11)}$$

where E_{cm} is the kinetic energy in the center of mass system, B_c is Coulomb barrier and $T(b)$ is the transparency function at impact parameter b.

In the OLA the $T(b)$ is written as [30]

$$\boldsymbol{T(b) = \left|S_{el}^{OL}(b)\right|^2,} \qquad \textbf{(12)}$$

where $S_{el}^{OL}(b)$ is the elastic $S-$matrix for the target-projectile system given as [30]:

$$\boldsymbol{S_{el}^{OL}(b) = exp[iO_{PT}(b)]} \qquad \textbf{(13)}$$

$$\boldsymbol{O_{PT}(b) = \int_{-\infty}^{\infty} dR_3 \int d\vec{r}_1 \int d\vec{r}_2 \rho_P(r_1)\rho_T(r_2) f_{NN}\left(\left|\vec{R} + \vec{r}_1 - \vec{r}_2\right|\right)} \qquad \textbf{(14)}$$

is the overlap of the ground state densities of projectile and target ($\rho_P$and ρ_T, respectively).

Results and discussion

The BCM is used to analyze the features of ground state such as neutron, proton and matter densities and elastic form factors for the proton-rich ^{23}Al $\left(S_p = 0.141 \text{ MeV}, \tau = 470\, ms\right)$ and ^{27}P $\left(S_p = 0.87 \text{ MeV}, \tau = 260\, ms\right)$ [37, 38] exotic nuclei. Two density parameterizations are used in BCM calculations namely; GS and

HO parameterizations. Moreover, the Glauber model is used to calculated the matter rms radii and σ_R of these exotic nuclei.

An important concept of a halo is the decoupling of the halo wave function from the core of the nucleus. Cluster models, which assume a halo nucleus to be a core plus halo nucleon (s), have been successful in most cases to describe halo nuclei [39].

The nuclei ^{23}Al $(J^{\pi}, T = 1/2^{+}, 3/2)$ and ^{27}P $(J^{\pi}, T = 1/2^{+}, 3/2)$ are composed of an inert cores ^{22}Mg $(J^{\pi}, T = 0^{+}, 1)$ and ^{26}Si $(J^{\pi}, T = 0^{+}, 1)$ plus one loosely bound proton, consecutively. In the HO parameterization, the density distributions of the core and halo clusters are parameterized with HO wave function. The core nuclei ^{22}Mg and ^{26}Si have the configurations $\{(1s_{1/2})^4, (1p_{3/2})^8, (1p_{1/2})^4, (1d_{5/2})^6\}$ and $\{(1s_{1/2})^4, (1p_{3/2})^8, (1p_{1/2})^4, (1d_{5/2})^{10}\}$, respectively. The outer proton of ^{23}Al and ^{27}P is assumed to have mixed configuration of $1d_{3/2}$ and $2s_{1/2}$ using the following relation [40]:

$$\boldsymbol{\rho_v = \left\{ \alpha \left| \phi_{2s_{1/2}} \right|^2 + (1-\alpha) \left| \phi_{1d_{3/2}} \right|^2 \right\} \qquad (\alpha \leq 1)}$$

Where $\phi_{2s_{1/2}}$ and $\phi_{1d_{3/2}}$ refer to the halo neutron wave functions of $2s_{1/2}$ and $1d_{3/2}$ with occupation probabilities 0.6 (in $2s_{1/2}$) and 0.4 (in $1d_{3/2}$) for the halo proton, respectively and α refer to the occupation probability of the $(2s_{1/2})$ orbital.

In the GS parameterization, the density distributions of the core and halo clusters are parameterized with Gaussian wave function. The GS and HO size parameters utilized in these calculations for exotic nuclei are calculated by Eq.(6) and summarized in Table 1, whereas those of stable nuclei ^{27}Al and ^{31}P are chosen to reproduce the experimental proton rms radii for these nuclei and presented in Table 2.

Table 1: GS and HO size parameters for the core and halo clusters.

Halo Nucleus	Core nucleus	GS		HO	
		$\hat{a}_c$ (fm)	$\hat{a}_v$ (fm)	$\hat{b}_c$ (fm)	$\hat{b}_v$ (fm)
^{23}Al	^{22}Mg	2.281	5.694	1.714	3.839
^{27}P	^{26}Si	2.411	4.731	1.868	3.248

Table 2: GS and HO size parameters for the stable nuclei ^{27}Al and ^{31}P.

Stable nucleus	α **(fm)**	b **(fm)**	$\langle r_p^2 \rangle_{cal}^{1/2}$**(fm)**		$\langle r_p^2 \rangle_{exp}^{1/2}$ **(fm) [41]**
			Gaussian	HO	
^{27}Al	2.474	1.835	3.03	3.03	3.03±0.02
^{31}P	2.605	1.896	3.19	3.19	3.19±0.03

Fig.2 illustrates the contributions of the core nucleons (green curve) and the valence proton (blue curve) to the matter density (dashed-dot red curve) for halo nuclei ^{23}Al and ^{27}P obtained by the GS (left part) and HO (right part) parameterizations along with their experimental matter density (gray area) [42, 43]. The top and bottom panels correspond to halo nuclei ^{23}Al and ^{27}P, respectively. The halo nucleus distinctive property (*i.e.* the long tail behavior) is revealed in all dashed-dot red curves of Fig. 2 which agree well with experimental data.

Fig.3 displays the densities of matter (dashed-dot red curve), neutron (blue curve), and proton (green curve). The long tail is the property that clearly revealed in the proton density (green curves) because it is found in the halo orbits. The steep slope behavior is clearly seen in the neutron density (blue curves) since the neutrons are absent in the halo orbit and all the neutrons of these nuclei are located in their cores.

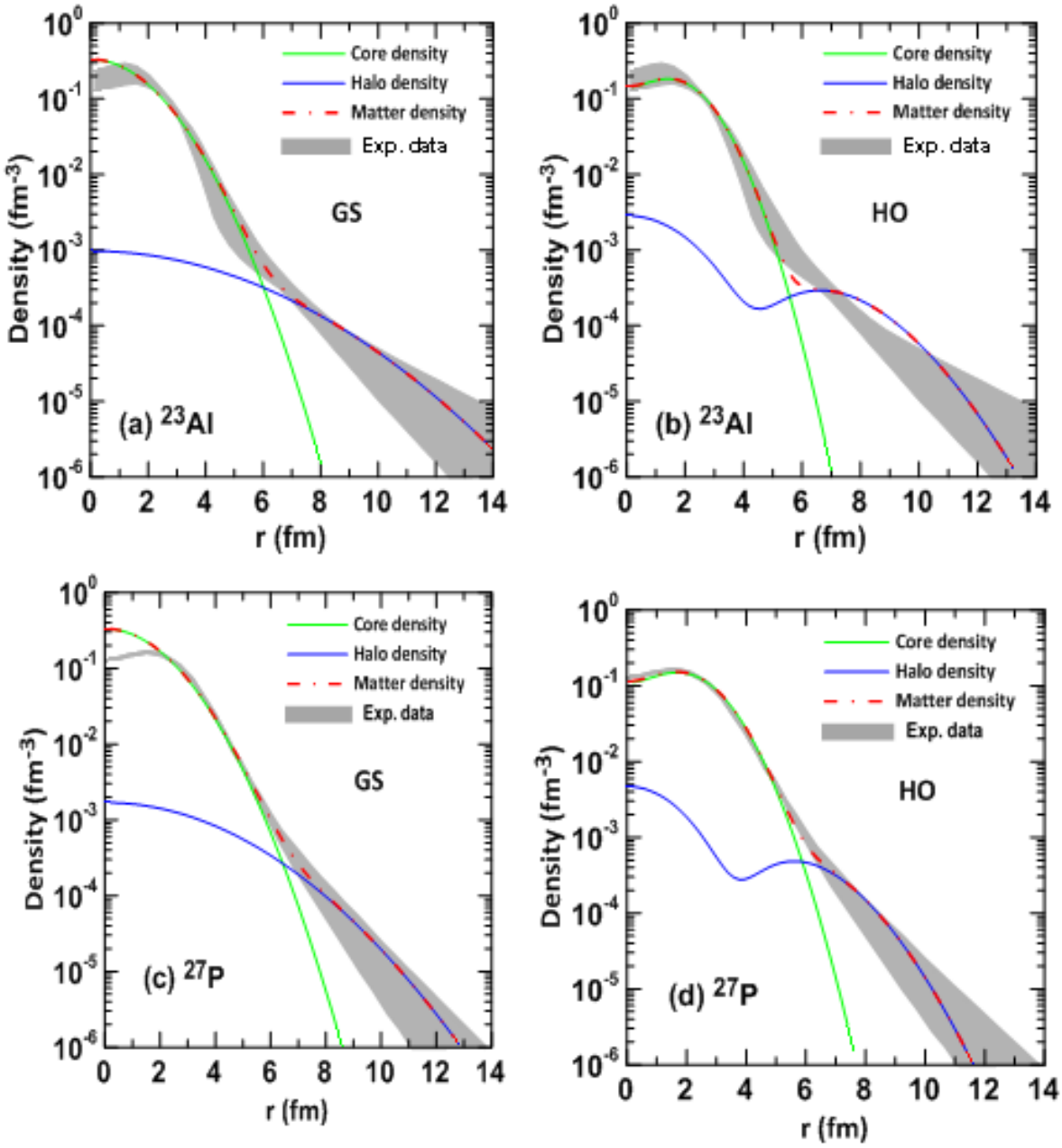

Fig. 2: The core, halo and matter density distributions for halo nuclei ^{23}Al and ^{27}P.

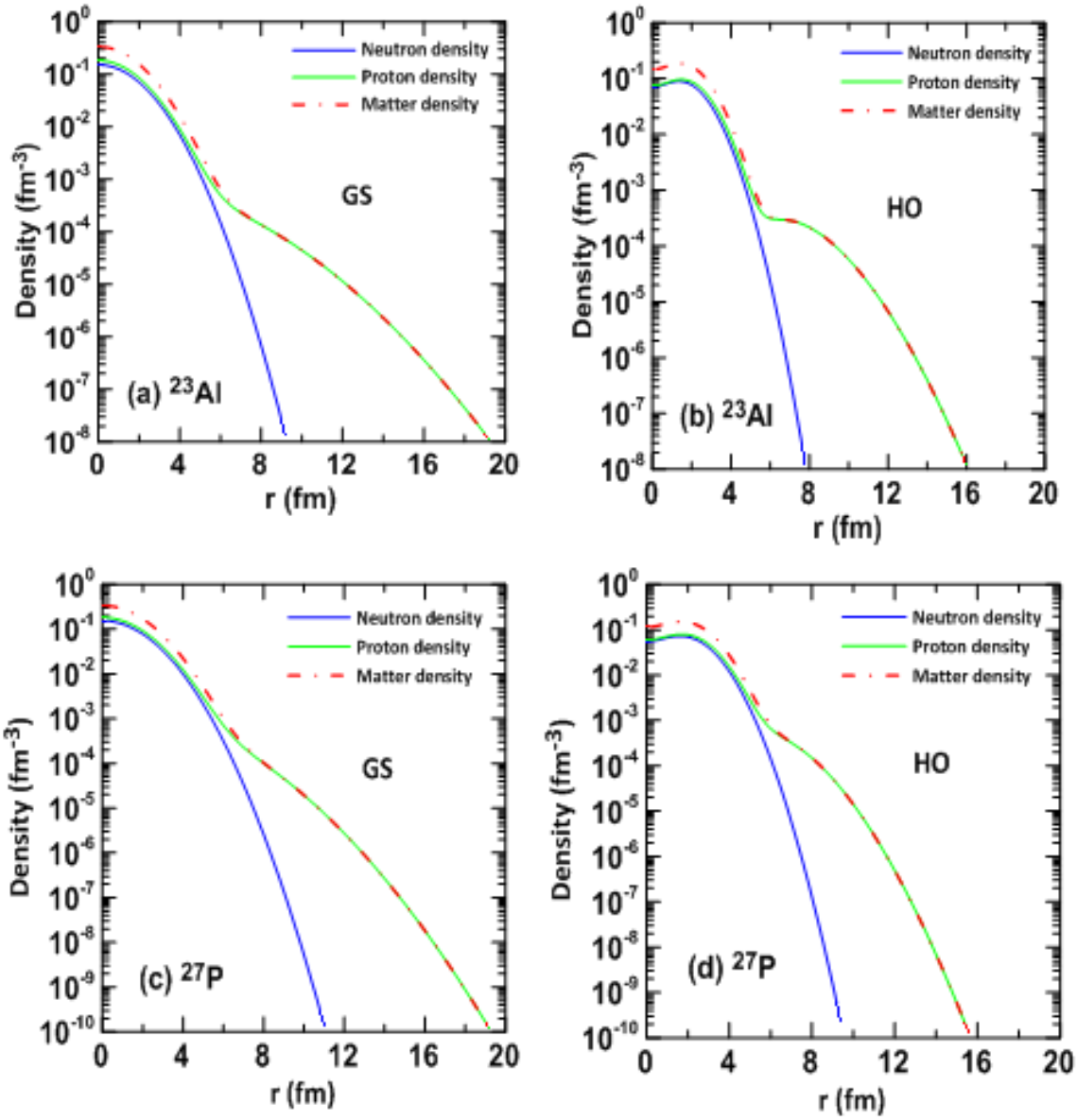

Fig. 3: The neutron, proton and matter density distributions for halo nuclei ^{23}Al and ^{27}P.

Fig.4 presents the proton density distributions for the isotopes pair ^{27,23}Al (top panel) and ^{31,27}P (bottom panel) calculated by the two density parameterizations. The proton densities of unstable and stable nuclei are plotted with green and dashed-dot red curves, consecutively. From these figures, it can be seen that the proton density distributions for each isotopes pairs are different although they have the same number of the protons.

The weak binding of the outer proton in exotic ^{23}Al and ^{27}P nuclei leads to the extended proton density distributions in them. So the last proton in ^{23}Al and ^{27}P plays a great role in density distribution and leads to exotic structure.

To find out if the long tail of the proton density distributions for the proton-rich nuclei displays observable effects in the process of elastic electron scattering, the longitudinal $C0$ elastic form factors for the proton-rich exotic nuclei ^{23}Al and ^{27}P (the red curves) and their stable isotopes ^{27}Al and ^{31}P (the green curves) calculated by PWBA with the proton densities obtained by HO method were plotted as shown in Fig.5. For comparison the experimental data of the stable isotopes ^{27}Al [44] and ^{31}P

[45] are portrayed by dotted symbols. It is obvious that the form factors for each isotopes pairs are quite different although they have the same proton number. The minima position of the red curve has right shift as compared with that of the green curve.

It is known that the elastic proton form factor of a nucleus is directly related to its proton density distribution. Therefore, the difference between the form factor of unstable nucleus ^{23}Al and that of its stable isotope ^{27}Al is due to the different proton density distributions of the two nuclei. Since the difference of the proton density distribution between ^{23}Al and ^{27}Al is mainly caused by the difference of the proton density distribution of the last proton in ^{23}Al and ^{27}Al, it can be concluded that the difference between the form factor of ^{23}Al and that of ^{27}Al indicates the difference in the density distribution of the last proton in the two nuclei. The same conclusion can be drown by similar argument for the nuclei ^{27}P and ^{31}P. Therefore, the elastic electron scattering is a powerful tool to investigate proton halo phenomena of proton-rich nuclei because the difference of the proton form factors between unstable (halo) nuclei and their stable isotopes has observable effects.

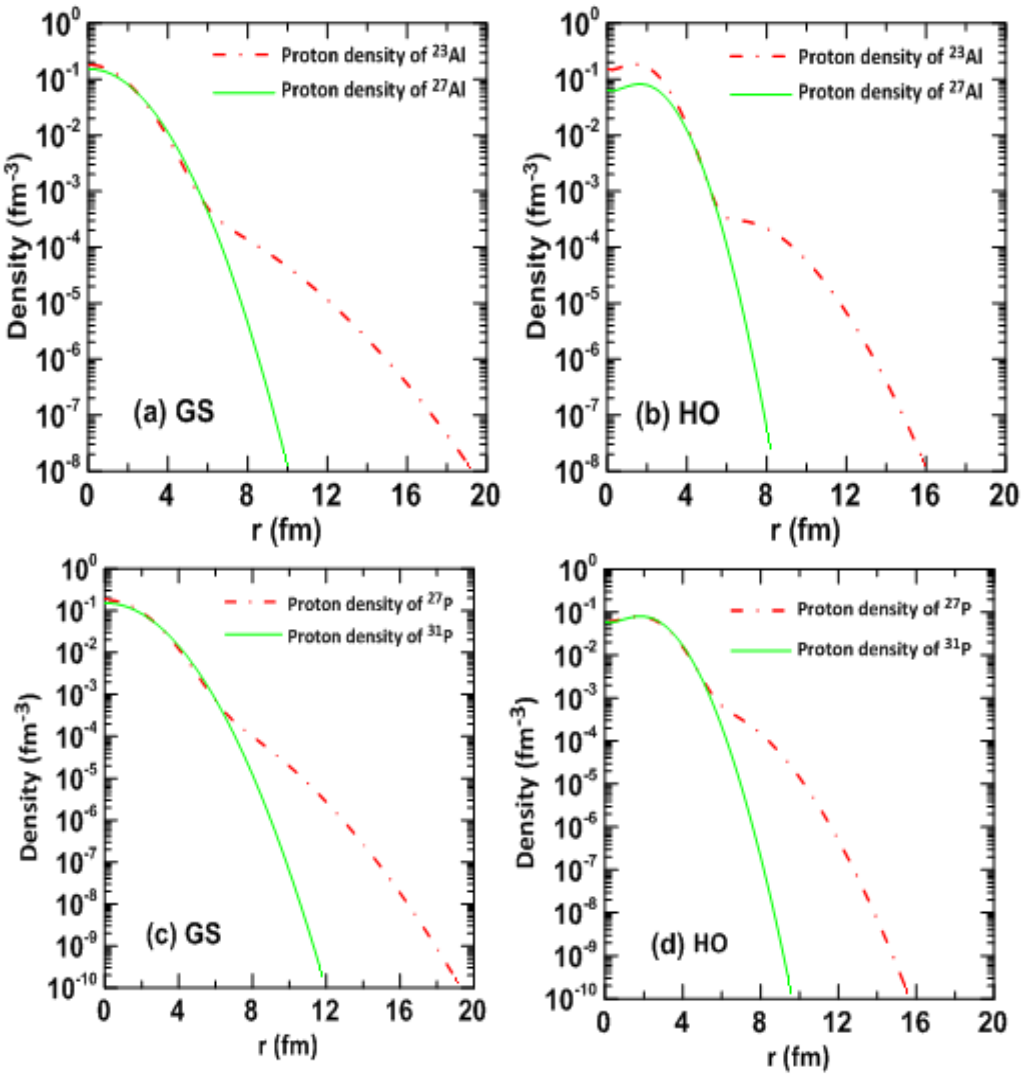

Fig. 4: The proton density distributions for isotopes pairs ^{27,23}Al and ^{31,27}P.

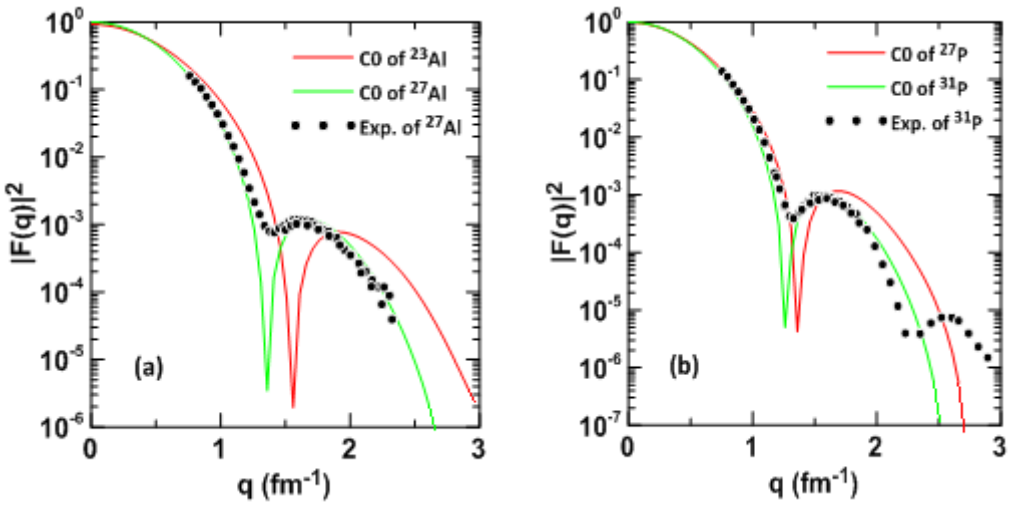

Fig. 5: The elastic form factors for isotopes pairs ^{27,23}Al and ^{31,27}P.

The σ_R were studied by means of the Glauber model with OLA at high and low energies for ^{23}Al and ^{27}P projectiles incident on the ^{12}C target using the ground state densities of these nuclei. The densities of the projectile and target were described by the single Gaussian functions with range parameters α_P and α_T for projectile and target nuclei, respectively. The calculated σ_R along with the corresponding experimental data [35] are listed in Table 3 and plotted in Fig.6. The open red and filled blue circle symbols are the calculated and experimental results, consecutively. From the results, one can see clearly that a good description of the experimental σ_R is obtained by the calculated results for both halo nuclei at high and low energies.

Table 3: Calculated and experimental σ_R for ^{23}Al+^{12}C and ^{27}P+^{12}C systems.

Halo nuclei	Energy (MeV) [46]	Calculated σ_R (mb)	Experimental σ_R (mb) [46]
^{23}Al	950	1220	1208±68
	36	1904	1892± 45
^{27}P	950	1240	1229±18
	33	2099	2089±119

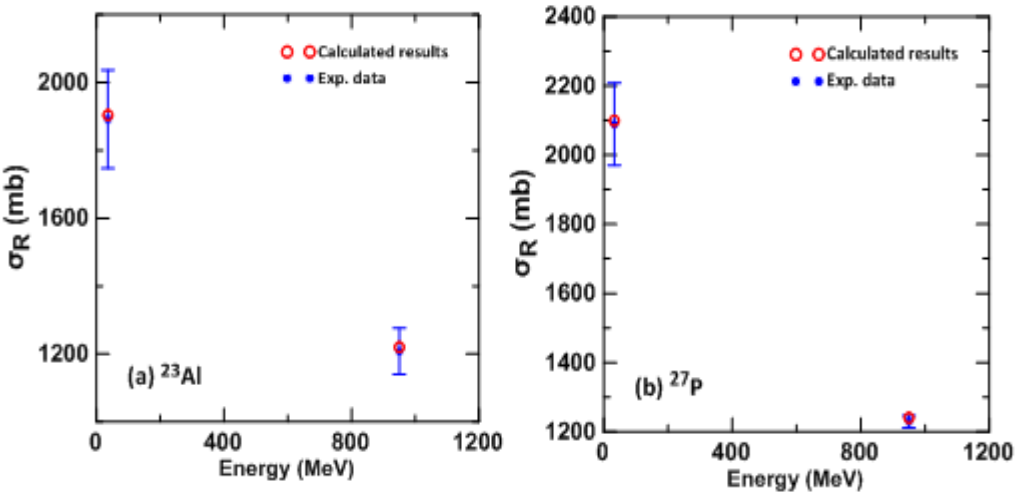

Fig. 6: The experimental and calculated results of reaction cross section for halo nuclei ^{23}Al and ^{27}P on ^{12}C target.

To calculate the matter rms radius of halo nuclei from the reaction cross sections (σ_R), the calculated σ_R (black line) obtained by the Glauber model within OLA versus the matter rms radii for the halo nuclei ^{23}Al and ^{27}P on ^{12}C target at energy 950 were plotted as shown in Fis.7(a andb), consecutively. The horizontal blue line shows the experimental σ_R (given in Table 3) with error bar represented by the shaded area. The intersection point of the black line with horizontal blue line represents the obtained matter rms radius ($\langle r_m^2 \rangle^{1/2}$) for the halo nuclei. It is obvious from Fig.7 that the calculated $\langle r_m^2 \rangle^{1/2}$ for ^{23}Al and ^{27}P are equal to 2.92 and 2.99 fm ,respectively which agrees well with the analogous experimental data of the values 2.905±0.25 and 3.02±0.15 fm [46].

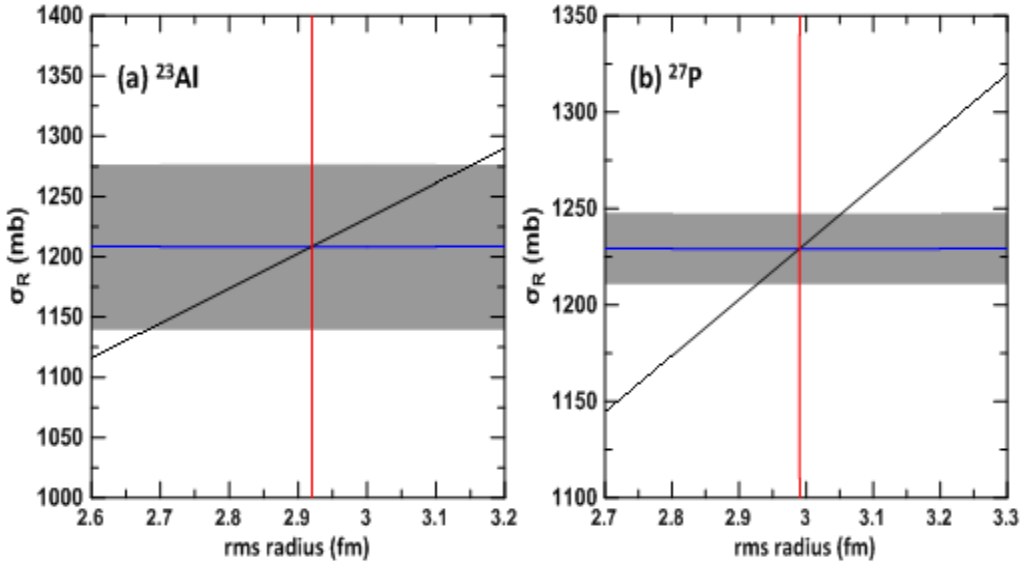

Fig. 7: The reaction cross section versus the matter rms radii for the halo nuclei ^{23}Al and ^{27}P.

Conclusions

According to the calculated results it was found:

The BCM within the Gaussian and harmonic oscillator wave functions is remarkably capable of providing theoretical predictions on the structure of halo nuclei and be in a satisfactory description with those of experimental data. The halo structure of ^{23}Al and ^{27}P exotic nuclei was emphasized through exhibiting the long tail performance in their calculated proton and matter density distributions, where this performance is considered as a distinctive feature of halo nuclei. The steep slope behavior was obviously seen in the calculated proton density distributions of considered halo nuclei, as a result of the absence of protons in halo orbits, where all protons are found in their cores only. The results of the matter density distributions calculations when the halo proton in ^{23}Al and ^{27}P has mixed configuration of (1*d*3/2) and (2*s*1/2) with dominant (2*s*1/2) were in best agreement with experimental data.

Calculations showed that the major difference between the elastic proton form factors of halo nuclei and those of their stable isotopes is caused by the variation in the proton density distributions, especially the details of the outer parts. Therefore, the elastic electron scattering is a powerful tool to investigate proton halo phenomena of proton-rich nuclei because the difference of the proton form factors between unstable (halo) nuclei and their stable isotope has observable effects. The Glauber model at high energy give a good description for both matter rms radii and σR of these nuclei.

Acknowledgment

The authors would like to thank everyone who supported them to complete this work.

References

[1] I. Tanihata, H. Hamagaki, O.Hashimoto, Y. Shida, N. Yoshikawa, K. Sugimoto, O. Yamakawa, T.Kobayashi, N. Takahashi, Phys. Rev. Lett., 55 (1985) 2676-2679.
[2] P. G. Hansen and B. Jonson, Euro. Phys. Lett., 4 (1987) 409-414.
[3] T. Nakamura, N. Kobayashi, Y. Kondo, Y. Satou, N. Aoi, H. Baba, S. Deguchi, N. Fukuda, J. Gibelin, N. Inabe, M. Ishihara, Phys. Rev. Lett., 103 (2009) 262501.
[4] Z. Wang and Z. Z. Ren, Sci. China G, Phys. Astron., 47 (2004) 42.
[5] B. Blank, C. Marchand, M.S. Pravikoff, T. Baumann, F. Boué, H. Geissel, M. Hellström, N. Iwasa, W. Schwab, K. Sümmerer, M. Gai, Nucl. Phys. A, 624 (1997) 242-256.
[6] T. Nilsson, F. Humbert, W. Schwab, H. Simon, M. H. Smedberg, M. Zinser, et al., Nucl. Phys. A, 598 (1996) 418-434.
[7] M. Zinser, F. Humbert, T. Nilsson, W. Schwab, Th. Blaich, M. J. G. Borge, L.V. Chulkov, H. Eickhoff, Th. W. Elze, H. Emling, B. Franzke, et al., Phys. Rev. Lett., 75 (1995) 1719-1722.
[8] N. A. Orr, N. Anantaraman, Sam M. Austin, C. A. Bertulani, K Hanold, J. H. Kelley, D. J. Morrissey, B. M. Sherrill, G. A. Souliotis, M.Thoennessen, J. S. Winfield, J. A. Winger, Phys. Rev. Lett., 69 (1992) 2050 -2053.
[9] R. Anne, S.E. Arnell, R. Bimbot, H. Emling, D. Guillemaud-Mueller, P.G. Hansen, L. Johannsen, B. Jonson, M. Lewitowicz, S. Mattsson, A.C. Mueller, Phys. Lett. B, 250 (1990) 19-23.
[10] Z. Ren and G. Xu, Phys. Lett. B, 252 (1990) 311-313.
[11] G. F. Bertsch and H.Esbensen, Ann., Phys. (N.Y.), 209 (1991) 327-363.
[12] P. G. Hansen, A. S. Jensen, B. Jonson, Annu. Rev. Nucl. Part. Sci., 45 (1995) 591-599.
[13] J. S. Al-khalili, J. A. Tostevin, I. J. Thompson, Phys. Rev. C, 54 (1996) 1843-1852.
[14] Z. Ren, B. Chen, Z. Ma, G. Xu, Phys. Rev. C, 53 (1996) 572-575.
[15] B. A. Brown, P. G. Hansen, Phys. Lett. B, 381 (1996) 391-396.
[16] Y.L. Parfenova, M.V. Zhukov, Phys. Rev. C, 66 (2002) 064607-1_064607-9.
[17] M.V. Zhukov, I.J. Thompson, Phys. Rev. C, 52 (1995) 3505-3058.
[18] A. Navin, D. Bazin, B.A. Brown, B. Davids, G. Gervais, T. Glasmacher, K. Govaert, P.G. Hansen, M. Hellström, R.W. Ibbotson, V. Maddalena, Phys. Rev. Lett., 81 (1998) 5089.
[19] H.Y. Zhang, W.Q. Shen, Z.Z. Ren, Y.G. Ma, W.Z. Jiang, Z.Y. Zhu, X.Z. Cai, D.Q. Fang, C. Zhong, L.P. Yu, Y.B. Wei, Nucl. Phys. A, 707 (2002) 303-324.
[20] Z. Li, W. Liu, X. Bai, Y. Wang, G. Lian, Z. Li, S. Zeng, Phys. Lett. B, 527 (2002) 50-54.
[21] I. Tanihata, H. Hamagaki, O. Hashimoto, S. Nagamiya, Y. Shida, N. Yoshikawa, O. Yamakawa, K. Sugimoto, T. Kobayashi, D.E. Greiner, N. Takahashi, Phys. Lett. B, 160 (1985) 380-384.
[22] I. Tanihata, D. Hirata, T. Kobayashi, S. Shimoura, K. Sugimoto, H. Toki, Phys. Lett. B, 289 (1992) 261-266.
[23] A. Ozawa, Nucl. Phys. A, 738 (2004) 38-44.
[24] Y. Ogawa, K. Yabanab, Y. Suzuki, Nucl. Phys. A, 543 (1992) 722-750.

[25] A. Ozawa, T. Baumann, L. Chulkov, D. Cortina, U. Datta, J. Fernandez, H. Geissel, F. Hammache, K. Itahashi, M. Ivanov, R. Janik, Nucl. Phys. A, 709 (2002) 60-72.
[26] A. A. Alzubadi, N. F. Latooffi, R. A. Radhi, Int. J. Mod. Phys. E, 24, 12 (2015) 1550099.
[27] Z. Ren, X.Z. Cai, H.Y. Zhang, W.Q. Shen, Physics of Atomic Nuclei, 66 (2003) 1515-1518.
[28] R. A. Radhi, G. N. Flaiyh, E. M. Raheem, Iraqi Journal of Physics, 13, 26 (2015) 12-28.
[29] A. N. Abdullah, Iran. J. Sci. Technol. Trans. Sci., 44 (2020) 283-288.
[30] J. A. Tostevin, R. C. Johnson, J. S. Al-Khalili, Nucl. Phys. A, 630 (1998) 340-351.
[31] A. K. Hamoudi and A. N. Abdullah, Iraqi Journal of Science, 57 (2016) 2664-2676
[32] A. N. Abdullah, Indian Journal of Natural Sciences, 8, 48 (2018) 13898- 13905.
[33] A. N. Abdullah, Int. J. Mod. Phys. E, 29 (2020) 2050015-1_2050015-10.
[34] A. N. Antonov M. K. Gaidarod. N. Kadrev, P. E. Hodgson, E. Moya de gurra Int. J. Mod. Phys. E, 13 (2004) 759-772.
[35] Z. Y. Lin, M. Z. Yu, C. B. Qiu, Commun. Theor. Phys., 36 (2001) 313-320.
[36] T. Zheng, T. Yamaguchi, A. Ozawa, M. Chiba, R. Kanungo, T. Kato, K. Katori, K. Morimoto, T. Ohnishi, T. Suda, I. Tanihata, Nucl. Phys. A, 709 (2002) 103-118.
[37] G. Audi, F.G. Kondev, Meng Wang, W.J. Huang, S. Naimi, Chin. Phys. C, 41, 3 (2017) 030001-1_030001-17.
[38] M. Wang, G. Audi, F.G. Kondev, W.J. Huang, S. Naimi, Xing Xu, Chin. Phys. C, 41, 3 (2017) 030003-1_030003-5.
[39] I. Tanihata, H. Savajols, R. Kanungo, Prog. Part. Nucl. Phys., 68 (2013) 215-313.
[40] Y. Yamaguchi, T. Suzuki, T. Ohtsubo, T. Izumikawa, W. Shinozaki, M. Takahashi, R. Koyama, S. Watanabe, C. Wu, A. Ozawa, T. Ohnishi, A New Era of Nucl. Stru. Phys., (2004) 114-118.
[41] H. D. Vries, C.W. Jager, C. Vries, Ato. dat. and Nucl. Dat. Tab., 36 (1987) 495-536.
[42] D.Q. Fang, C.W. Ma, Y.G. Ma, X.Z. Cai, J.G. Chen, J.H. Chen, W. Guo, W.D. Tian, K. Wang, Y.B. Wei, T.Z. Yan, Chin. Phys. Lett., 22 (2005) 572-575.
[43] D.Q. Fang, W.Q. Shen, J. Feng, X.Z. Cai, H.Y. Zhang, Y.G. Ma, C. Zhong, Z.Y. Zhu, W.Z. Jiang, W.L. Zhan, Z.Y. Guo, The Eur. Phys. J. A-Hadr. and Nucl., 12, 3 (2001) 335-339.
[44] G. C. Li, M. R. Yearian, I. Sick, Phys. Rev. C, 9 (1974) 1861-1877.
[45] B.B.P. Sinha, G.A. Peterson, G.C. Li, R.R. Whitney, Physical Review C, 6, 5 (1972) 1657-1663.
[46] H.Y. Zhang, W.Q. Shen, Z.Z. Ren, Y.G. Ma, W.Z. Jiang, Z.Y. Zhu, X.Z. Cai, D.Q. Fang, C. Zhong, L.P. Yu, Y.B, Wei, Nuclear Physics A, 707, 3-4 (2002) 303-324.